Thermal Science and Engineering 2024, 7(3), 9102.
https://doi.org/10.24294/tse.v7i3.9102

Article

Enhancement of heat dissipation efficiency in the CSNS target through the innovative design of a serial cooling water channel

Jiahui Chen[1,2,3], Jianfei Tong[2,3,*], Youlian Lu[2,3], Songlin Wang[2,3], Tianjiao Liang[2,3], Jian Wen[1]

[1] School of Energy and Power Engineering, Xi'an Jiaotong University, Xi'an 710049, China
[2] Institute of High Energy Physics, Chinese Academy of Sciences (CAS), Beijing 100049, China
[3] Spallation Neutron Source Center, Dongguan 523803, China
*** Corresponding author:** Jianfei Tong, tongjf@ihep.ac.cn

CITATION

Chen J, Tong J, Lu Y, et al. Enhancement of heat dissipation efficiency in the CSNS target through the innovative design of a serial cooling water channel. Thermal Science and Engineering. 2024; 7(3): 9102. https://doi.org/10.24294/tse.v7i3.9102

ARTICLE INFO

Received: 12 September 2024
Accepted: 25 September 2024
Available online: 30 September 2024

Abstract: This paper presents a coupling of the Monte Carlo method with computational fluid dynamics (CFD) to analyze the flow channel design of an irradiated target through numerical simulations. A novel series flow channel configuration is proposed, which effectively facilitates the removal of heat generated by high-power irradiation from the target without necessitating an increase in the cooling water flow rate. The research assesses the performance of both parallel and serial cooling channels within the target, revealing that, when subjected to equivalent cooling water flow rates, the maximum temperature observed in the target employing the serial channel configuration is lower. This reduction in temperature is ascribed to the accelerated flow of cooling water within the serial channel, which subsequently elevates both the Reynolds number and the Nusselt number, leading to enhanced heat transfer efficiency. Furthermore, the maximum temperature is observed to occur further downstream, thereby circumventing areas of peak heat generation. This phenomenon arises because the cooling water traverses the target plates with the highest internal heat generation at a lower temperature when the flow channels are arranged in series, optimizing the cooling effect on these targets. However, it is crucial to note that the pressure loss associated with the serial structure is two orders of magnitude greater than that of the parallel structure, necessitating increased pump power and imposing stricter requirements on the target container and cooling water pipeline. These findings can serve as a reference for the design of the cooling channels in the target station system, particularly in light of the anticipated increase in beam power during the second phase of the China Spallation Neutron Source (CSNS II).

Keywords: CSNS target; heat dissipation; Monte Carlo method; serial flow; CFD; pump power

1. Introduction

As a kind of multidisciplinary platform for scientific research, spallation neutron sources have garnered increasing attention in recent years. Its applications span various fields, including basic-energy sciences, nuclear science, and the utilization of white neutrons/fast neutrons, as well as proton beam applications and meson research [1,2]. The neutron flux produced by a spallation neutron source serves as a critical metric for evaluating its operational efficiency; however, achieving a higher neutron flux necessitates an increase in beam power, which consequently results in elevated heat generation at the target station [3]. Thus, the development of effective heat removal strategies is of paramount importance for enhancing the power capabilities of spallation neutron sources.

A variety of heat removal techniques have been reported to be implemented in spallation neutron source targets globally. Spallation Neutron Source (SNS) in the United States and the Japan Proton Accelerator Research Complex (J-PARC) Pulsed Spallation Neutron Source (JSNS) are both megawatt-class neutron sources that utilize liquid mercury as coolant within the target [4,5]. The target of the Swiss Spallation Neutron Source (SINQ) in Switzerland employs an array of target rods that contain a sealed liquid lead-bismuth alloy [6]. The European Spallation Neutron Source (ESS), currently under construction, is also designed as a megawatt-level neutron source, featuring a large wheel-shaped target vessel [7]. The target configuration in Target Station 1 (TS-1) of Neutron and Muon Source at the Rutherford Appleton Laboratory in the United Kingdom consists of a fragmented target with integrated parallel cooling channels [8]. Analogous to ISIS TS-1 target, the target employed in the China Spallation Neutron Source (CSNS) in also characterized as a segmented target with parallel cooling channel [9]. This configuration is specifically developed to enhance cooling through a parallel flow system, which comprises a single inlet and a single outlet.

Among the aforementioned targets, the interaction of proton pulses with the liquid mercury target will generate pressure wave phenomena, which may result in a deleterious effect known as cavitation damage erosion [10]. Additionally, the polonium isotopes that are difficult to handle will occur in the Pb-Bi eutectic target as a consequence of irradiation, and the sealing of the target rod is also challenging [7,11]. Furthermore, rotating targets present issues related to duty cycles, and the target material is subjected to significant thermal cycling, potentially leading to embrittlement of the material [7]. Consequently, a mature design with solid fixed targets remains the preferred option for CSNS targets.

The utilization of parallel channels is prevalent in the majority of current solid fixed targets designed for heat dissipation. Research conducted by Hao Junhong et al. [12,13] focused on the thermal management of spallation neutron source targets, while Lu [14] examined the impact of proton beam deviation on the heat dissipation efficacy of the spallation neutron source target. Additionally, Allen and Findlay et al. investigated the decay heat with the target at the ISIS TS-1 facility. Takenaka [15] analyzed the parallel flow channels in megawatt-level sliced targets and target rod arrays, concluding that the minimum thickness of the target slice should be less than 9 mm. Bauer [16] similarly asserted that in spallation neutron sources operating at elevated proton beam power, the minimum gap size between targets may need to be reduced to below 0.7 mm. Furthermore, in addressing multi-channel cooling challenges, the effective delivery and distribution of coolant are critical for optimizing cooling performance [17]. Kumar and Singh [18] emphasized that the configuration of flow and the actual distribution of coolant must align with the heat flow to enhance better heat dissipation efficiency. If the thickness of the target plates and the inter-plate gaps are excessively small, the number of parallel channels will increase and make it difficult for the distribution of the coolant. Additionally, overly diminutive dimensions may pose significant challenges in terms of processing and installation.

Currently, research on the parallel channels of solid fixed targets is relatively comprehensive, whereas investigations into the heat dissipation mechanism of serial channels within the targets remain limited. Consequently, this paper introduces a novel

serial flow channel designed for application in irradiated targets, informed by an analysis of the heat dissipation phenomena observed in complex flow channels at the CSNS. In the design of the serial flow channel, it is demonstrated that the dimensions of the target plates and flow channels do not significantly influence the distribution of the coolant. The cooling water can be effectively concentrated in regions exhibiting higher thermal power, thereby ensuring adequate cooling in those areas. This study examines the differences in heat dissipation between serial and parallel structures, evaluates the respective advantages and disadvantages of each configuration, and offers critical insights and recommendations for the enhancement of CSNS II.

2. CSNS target and simulation model

The structure of the current target utilized in CSNS is illustrated in **Figure 1**. The primary component consists of fifteen tantalum-clad tungsten target plates, which are installed within a stainless steel vessel. The design incorporates gaps ranging from 0.8 to 1.2 mm between the target plates to facilitate effective heat dissipation. Additionally, two stainless steel ribs are positioned among the target plates to provide structural reinforcement. Cooling water is introduced into the target vessel from one side, subsequently circulating the parallel channels formed between the target plates before exiting the vessel. Thermocouples are strategically installed in select plates to monitor the temperature of the target.

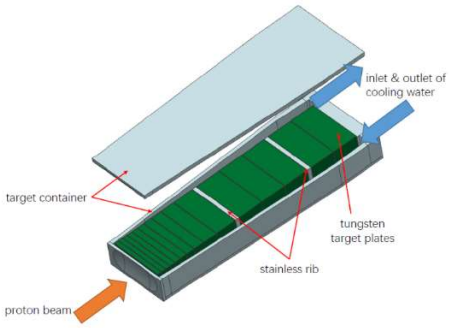

Figure 1. The structure of the CSNS target.

In the operational context, the target is bombarded by high-power proton beams, resulting in thermal energy deposition approximately equivalent to half of the beams' power within the target. Utilizing the Monte Carlo method, the energy deposited in the target is attributed to three primary mechanisms. The first mechanism is the energy loss associated with the ionization of electrons in atomic structures by protons and secondary charged particles, referred to as ionization energy loss. The second mechanism involves the recoil energy generated when fragments with elevated excitation energy release particles. The third mechanism pertains to the energy released during the fission of residual nuclei. This study integrates the Monte Carlo method with computational fluid dynamics (CFD). The heat deposition generated by proton interactions with the heavy metal target is calculated using Monte Carlo N-Particle Transport Code (MCNP), and this heat deposition is subsequently incorporated into FLUENT software as an internal heat source for thermal analysis. The distribution of generated heat within the target is non-uniform, as illustrated in

Figure 2. This figure depicts the model employed in MCNP and the spatial distribution of the internal heat source within the target when the proton beam power is set as 100 KW. It is evident that the majority of the heating power is concentrated in the target plates located at the front of the vessel.

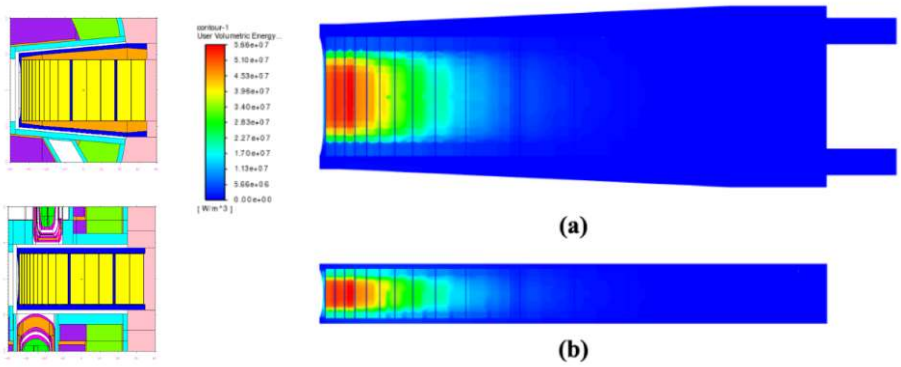

Figure 2. Model employed in MCNP and heat source power contour. **(a)** horizontal section; **(b)** vertical section. (protons delivered from left to right).

In order to maintain the maximum temperature of each target plate stay within the designated design parameters, the current target is cooled using water that circulates through the gaps between the target plates. This system allows for adjustments in both velocity and flow rate within each gap, a configuration referred to as a parallel channel. In this arrangement, the allocation of cooling water to regions with high heating power is critical in determining the overall efficiency of the target. Conversely, in a serial channel configuration, the channels are arranged sequentially, allowing for a concentration of cooling water in the areas of the target that experience higher power output.

In engineering practice, modifications to the target plates and channels can significantly impact the efficiency of heat dissipation in the target. Consequently, this paper presents a simplified structure of the target to mitigate the effects of such optimizations. **Figure 3** illustrates two channel models utilized in this study, where the gray region represents the target plate and the blue region denotes the cooling channel. Given that the majority of internal heating power is concentrated at the front of the vessel, there is an increased requirement for cooling in the target plates located in this region. As a result, the target plates are designed to be thicker in the direction of the proton beam. A detailed description of the channels is provided in **Figure 4**.

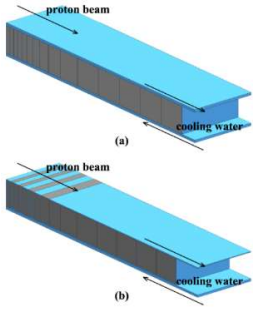

Figure 3. Model for simulation. **(a)** parallel channel configuration; **(b)** serial channel configuration.

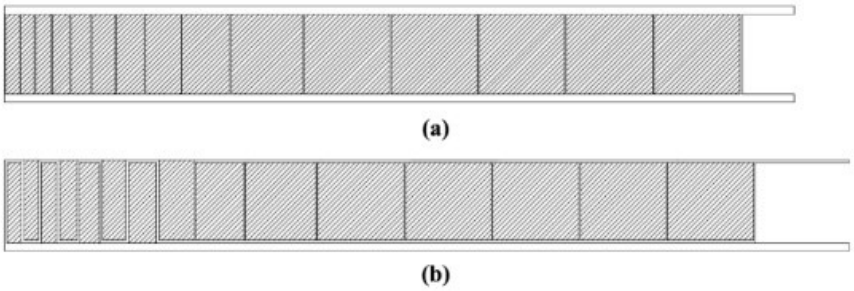

Figure 4. Cross section of the flow channel. **(a)** parallel channel configuration; **(b)**serial channel configuration.

In the parallel channel model, cooling water is introduced from one side of the target and exits from the opposite side after traversing through parallel channels. Conversely, the serial channel is implemented at the front 7 target plates, while the parallel configuration is maintained for the rear 8 target plates due to the reduced internal heat generation. The dimensions of the target plates and channels are presented in **Table 1**, which corresponds to the actual specifications. The inlet temperature of the cooling water is set at 28 ℃.

Table 1. The dimensions of the target plates and channels.

No. of target plate	Target plate thickness (mm)	No. of channel	Width of parallel channel (mm)	Width of serial channel (mm)
1	12.6	0	1	2.5
2	12.6	1	1	2.5
3	13.6	2	1	2.5
4	15.6	3	1	2.5
5	17.6	4	1	2.5
6	20.6	5	1	2.5
7	24.6	6	1	2.5
8	31.6	7	1	2.5
9	42.6	8	1	1
10	63.6	9	1	1
11	76.6	10	1	1
12	76.6	11	1	1
13	76.6	12	1	1
14	76.6	13	1	1
15	76.6	14	1	1
\		15	1	1

3. Results

Based on the actual process parameters, 8 cases have been studied in this paper for both models. The specifics of these cases are presented in **Table 2**, which serves solely for illustrative purposes. Detailed parameters will be attached with the analysis subsequently.

Table 2. List of cases.

Parallel channel model		**Cooling water flow rate (kg/s)**		
		2.3	2.5	2.7
Proton beam power (kW)	50	\	A3	\
	100	A1	A4	A2
	200	\	A5	\
	500	\	A6	\
	800	\	A7	\
	1000	\	A8	\
Serial channel model		**Cooling water flow rate (kg/s)**		
		2.3	2.5	2.7
Proton beam power (kW)	50	\	B3	\
	100	B1	B4	B2
	200	\	B5	\
	500	\	B6	\
	800	\	B7	\
	1000	\	B8	\

The subsequent analysis presents a comparison of temperature profiles between serial and parallel models. **Figure 5** illustrates the centerline temperature variations at a constant cooling water flow rate of 2.5 kg/s. The target plates, designated as 1 through 15, were aligned with the direction of the proton beam. It is evident that the temperature of target plates 1–10 in the serial model is lower than those observed in the parallel model. Conversely, the temperature of target plates 11–15 in the parallel model is comparatively lower. Furthermore, across all three scenarios examined, the peak temperature in the serial model occurs at target plate 9, whereas in the parallel model, it is observed at target plate 6. A comparison of the maximum target temperatures between the two models reveals that the maximum temperature in the parallel model consistently exceeds that of the serial model. When the proton beam power is increased to 1 megawatt (MW), the maximum temperature of the target in the parallel configuration is approximately 100 K higher than that in the serial configuration.

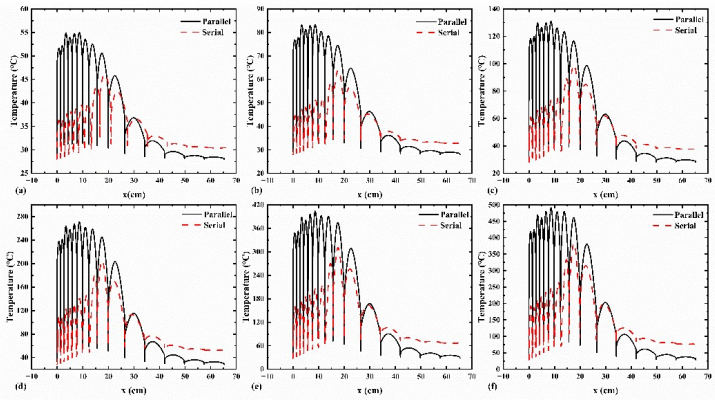

Figure 5. Profiles of the temperature along the centerline for different configurations under. **(a)** 50KW; **(b)** 100KW; **(c)** 200KW; **(d)** 500KW; **(e)** 800KW; **(f)** 1000KW.

Figure 6 presents a comparative analysis of the temperature distribution within the two distinct configurations. The legend for the temperature contours remains consistence across both configurations when subjected to the same proton beam power. Notably, the temperatures of the first 8 target plates in the serial configuration are significantly lower than those observed in the parallel model. This observation suggests that, for the initial 8 target plates with elevated internal heat generation, the heat produced can be dissipated more effectively through serial flow configurations. Conversely, for the subsequent 7 target plates, the temperature remains within the designated design parameters, attributable to the reduction in internal heat generation, despite a lower heat dissipation efficiency.

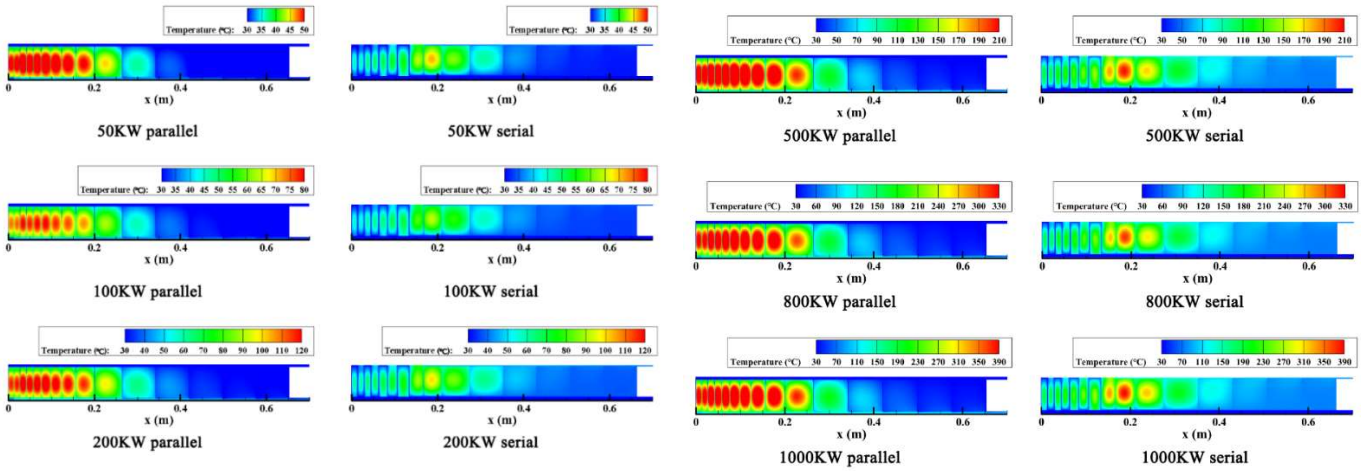

Figure 6. Temperature contours for parallel/serial configurations under different proton beam powers. **(a)** 50/100/200 KW; **(b)** 500/800/1000 KW.

Due to the significant temperature disparity observed between scenarios involving power levels exceeding 500 KW and those with lower power outputs, the subsequent analysis and discussions will be focused on power levels of 50 KW, 100 KW, and 200 KW to facilitate a more coherent examination.

Figure 7 illustrates the temperature profiles along the centerline of the model under varying proton beam power, with the cooling water flow rate maintained at 2.5 kg/s. Each line in the figure contains 15 peak values, which correspond to the maximum temperature recorded for each target plate. As depicted in **Figure 7(a)**, target plate 6 exhibits the highest temperature within the parallel model, with maximum temperatures of 55 ℃, 81 ℃ and 131 ℃ observed at proton beam powers of 50 KW, 100 KW, and 200 KW, respectively. This phenomenon can be attributed to the concentration of heating power in the target plates located at the front of the vessel, resulting in a temperature decline along the x-axis beyond plate 6. Conversely, **Figure 7(b)** indicates that in the serial configuration, the highest temperature is recorded on plate 9, with maximum temperatures of 46 ℃, 64 ℃ and 99 ℃ at the same proton beam powers. This suggests that the serial channel effectively enhances heat dissipation for the initial target plates. Furthermore, **Figure 8** presents the temperature profiles along the centerline under a fixed proton beam power of 100 KW. The data indicate that variations in the cooling water flow rate do not significantly alter the

trend of temperature change along the x-axis. Additionally, a 10% change in the cooling water flow rate has a minimal impact on the target temperature.

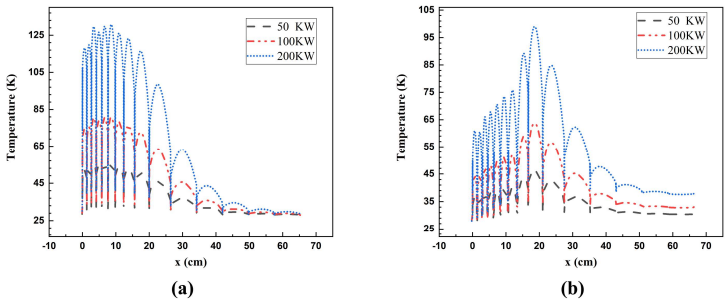

Figure 7. Profiles of temperature along the centerline for different proton beam power under cooling water flow rate of 2.5 kg/s. **(a)** parallel channel model; **(b)**serial channel model.

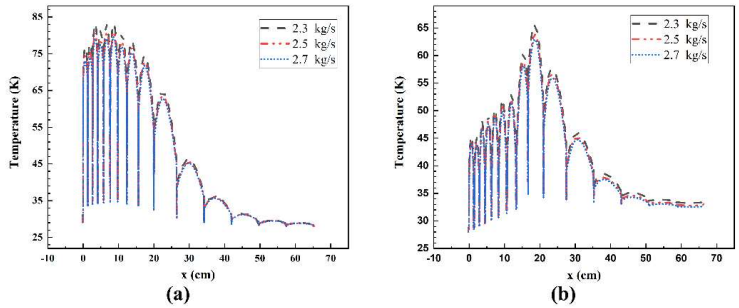

Figure 8. Profiles of the temperature along the centerline for different cooling water flow rates under the proton beam power of 100KW. **(a)** parallel configuration; **(b)** serial configuration.

4. Effect of structure on Nusselt Number

The dimensions of the channel and the flow rate within a serial model differ from those in a parallel model, even when subjected to identical cooling water flow rates and proton beam power. This inconsistency complicates the analytical process; therefore, the Nusselt Number (*Nu*) functions as a standardized metric that aids in this analysis.

$$Nu = \frac{hl}{\lambda} \tag{1}$$

where h is the convective heat transfer coefficient and l is the characteristic length defined as the width of the flow channel. λ is the thermal conductivity of the cooling water, which is evaluated at the average temperature within the flow channel. The initial channel positioned in the direction of the proton beam is designated as channel 0. **Figure 9** illustrates the *Nu* for each channel under varying proton beam power conditions. **Figure 9(a)** presents the *Nu* values for the parallel model, revealing that as the channel number increases, the *Nu* initially rises gradually before experiencing a rapid decline. Notably, the *Nu* values in the front channels are greater than those in the rear channels, indicating that the heat exchange efficiency is enhanced in the front channels due to a more significant temperature differential between the cooling water and the channel walls. **Figure 9(b)** depicts the *Nu* values for the serial model. Unlike

the parallel model, the peak value of *Nu* is observed within the channel 3–5, aligning with the target plates 3–6, which possess the highest internal heat source. Channels 9–15 are configured as parallel channels, resulting in a diminished flow rate. Concurrently, the temperature of the associated targets is expected to decrease as a result of the declining internal heat source. Consequently, *Nu* in channels 9–15 is considerably lower than that in the preceding channels. Furthermore, it is evident that the *Nu* value for the serial channel arrangement is markedly greater than that of the parallel arrangement under identical conditions, a difference that is particularly pronounced in the front channels.

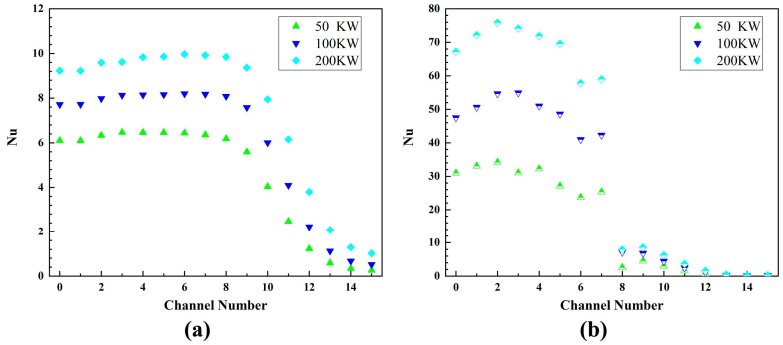

Figure 9. *Nu* in each channel under different proton beam power. **(a)** parallel channel configuration; **(b)** serial channel configuration.

Figure 10 illustrates the velocity of the cooling water(a) and the Reynolds number(b) within the channel, corresponding to a cooling water flow rate of 2.5kg/s.

$$Re = \frac{\rho v l}{\mu} \tag{2}$$

where ρ is the density of water within the channel, v is the average velocity of water in the channel, l is the characteristic length, which corresponds to the width of the flow channel, μ is the dynamic viscosity, and the characteristic temperature is defined as the average temperature of the cooling water in the channel. As illustrated in **Figure 10**, the flow velocity and Reynolds number (Re) of the cooling water in the serially arranged channels 0–7 are significantly greater than those recorded in the parallel configuration. This observation suggests a more intense forced convective heat transfer process occurring within the initial 8 flow channels, which is further corroborated by the data presented in **Figure 9**.

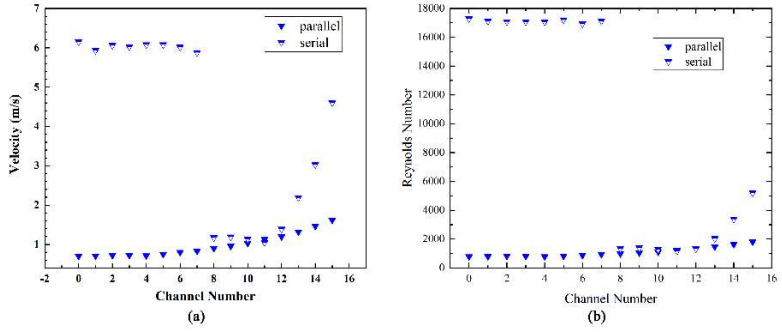

Figure 10. Comparison of Velocity. **(a)** and Reynolds number; **(b)** between two configurations with a cooling water flow rate of 2.5 kg/s.

Figure 11 presents a comparative analysis of the Nusselt number (*Nu*) in both parallel model and serial configurations under varying proton beam power with a cooling water flow rate of 2.5 kg/s. It is evident that the *Nu* values for channels 0–7 in the serial model are significantly greater than those observed in the parallel model, suggesting that the serial model exhibits superior heat transfer efficiency. Conversely, in channels 8–15, the parallel model demonstrates enhanced heat transfer efficiency. Given that the majority of the heating power is concentrated in the target plates located at the front end of the vessel, the distribution of *Nu* in the serial model is more effective in mitigating the maximum temperature of the target. This implies that the surface temperature of the target can be maintained within a safe range with a reduced volume of cooling water when utilizing the serial cooling channel configuration.

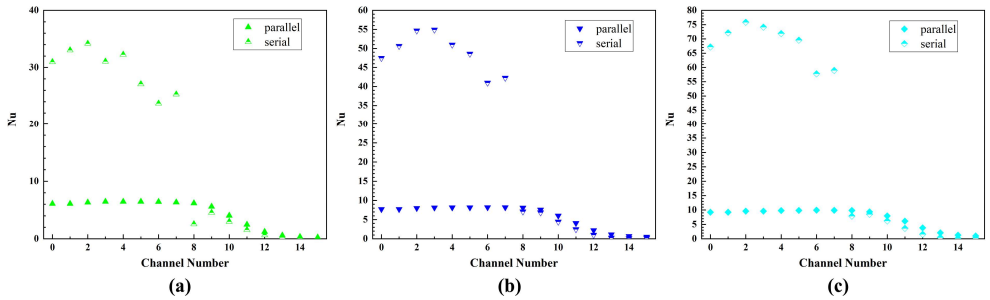

Figure 11. Comparison of *Nu* between two configurations with a cooling water flow rate of 2.5 kg/s. **(a)** 50KW; **(b)** 100KW; **(c)** 200KW.

In the serial model, the inlet of each channel is connected to the outlet of the preceding channel, resulting in an increase in water temperature as it progresses through each channel. This phenomenon may exacerbate the heat dissipation capabilities of the preceding channel. **Figure 12** illustrates a comparison of the average temperatures of the cooling water across various channels under differing proton beam power levels. In the parallel model, channels 0–7 exhibit similar average temperatures, with channels 3–6 displaying slightly elevated temperatures compared to the others. Conversely, the average temperatures in channels 8–15 are significantly lower. This discrepancy can be attributed to the independent flow characteristics of each channel in the parallel model, where the flow rates are relatively uniform (as shown in **Figure 10**). Therefore, the average temperature within each channel is influenced primarily by the internal heat sources of the target plates, leading to a temperature evolution that mirrors that of the target plates. In contrast, the average temperatures of channels 0–7 in the serial model demonstrate a linear increase. This trend arises from the direct connection between the inlet of each channel and the outlet of the preceding channel, resulting in a rise in the cooling water temperature as it flows through. Channels 8–15, being part of the parallel configuration, also exhibit temperature variations that correlate with the internal heat source power of the target plates. Given that the inlets of channels 8–15 effectively function as the outlets of channel 7, the minimum average temperature in these channels is inherently higher than that of channel 7. Obviously, the parallel flow configuration distributes the cooling capacity of the water by adjusting the flow to each channel, while the serial flow concentrates the cooling capacity at the front of the target. Since the heating power of the target is

predominantly concentrated in the front target plates, this characteristic of the serial configuration is particularly advantageous for reducing the temperature of the target at the front of the vessel.

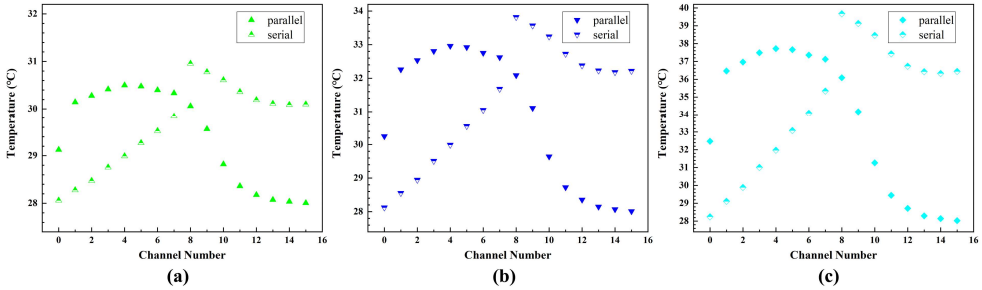

Figure 12. Comparison of the temperature measurements across each channel between two distinct configurations with a cooling water flow rate of 2.5 kg/s. **(a)** 50KW; **(b)** 100KW; **(c)** 200KW.

5. Effect of channel on pressure loss

The pressure loss within the channel and the power required by the pump serve as critical indicators of channel design. **Figure 13** illustrates the impact of cooling water flow rate on pressure loss (a) and pump power (b) across various models, specifically under conditions where the proton beam power is set at 100 KW. It is evident that, for a given cooling water flow rate, the pressure loss in a serial channel consistently exceeds a parallel channel. This phenomenon can be attributed to the parallel configuration, which distributes the cooling water flow across multiple channels, resulting in a larger cross-sectional area for the cooling water pathway. Consequently, the increase in pressure loss necessitates a significant rise in pump power.

$$P_{Pump} = \Delta PQ \tag{3}$$

where ΔP is the pressure loss within the target vessel, and Q is the flow rate of the cooling water. The relationship established by the formula indicates that pump power is directly proportional to pressure loss, a correlation that is substantiated by the data presented in **Figure 13(b)**. Furthermore, it is evident that in the serial configuration, both pressure loss and pump power exhibit a more pronounced increase with rising cooling water flow rates compared to the parallel configuration. **Figure 14** illustrates the effect of cooling water flow rate on the maximum temperature of the target across different configurations, specifically under conditions where the proton beam power is set as 100 KW. Consistent with the trends observed in pressure loss, the maximum temperature of the target in the serial model decreases more significantly with an equivalent increase in cooling water flow rate. Therefore, it can be concluded that the serial channel is more advantageous for heat dissipation; however, it also incurs greater pressure loss and pump power requirements. At low proton beam power levels, the cooling capacity of the parallel channel configuration is sufficient. Conversely, as the proton beam power increases, the serial design becomes more effective in enhancing heat dissipation, albeit at the expense of increased pump power.

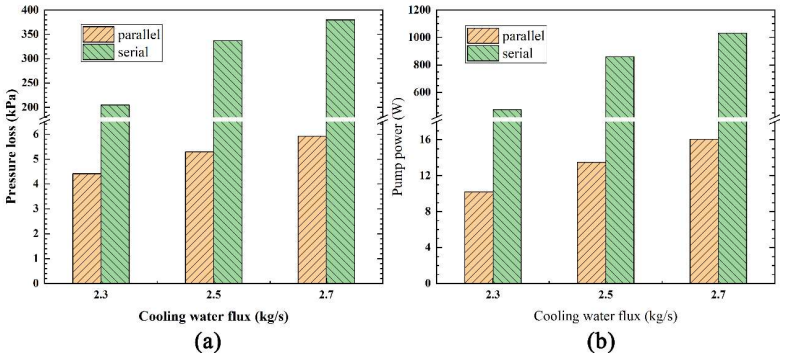

Figure 13. Influence of the cooling water flow rate on the pressure loss. **(a)** and the pump power; **(b)** in different configurations with the proton beam power of 100KW.

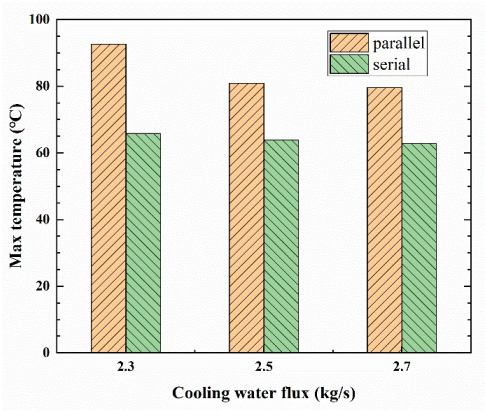

Figure 14. Influence of the cooling water flow rate on the maximum temperature of the target in different configurations with the proton beam power of 100KW.

6. Conclusion

This paper presents a numerical investigation of heat dissipation in a novel serial channel configuration within a solid fixed target, utilizing a combination of the Monte Carlo method and computational fluid dynamics (CFD). The implementation of a serial channel significantly enhances the cooling efficiency of the target, particularly under conditions where the flow of cooling water is constrained.

a) The flow rate of cooling water within the serial channel is elevated, resulting in increased Reynolds (Re) and Nusselt (Nu) numbers, which in turn enhances the heat transfer performance. Therefore, for a constant cooling water flow rate, the maximum temperature of the target equipped with the serial channel is reduced;

b) The serial design facilitates a decrease in the temperature of the cooling water as it traverses the initial target plates, thereby prioritizing the cooling of the high-power regions. This configuration results in the highest temperature point of the target being positioned further downstream, which is advantageous for managing the heat dissipation in structures characterized by uneven heat distribution, such as irradiated targets;

c) The introduction of a serial flow channel contributes to an increase in pressure within the target, necessitating greater pump power to circulate the coolant. This requirement imposes higher standards on the target container and the cooling water pipeline infrastructure.

Author contributions: Conceptualization, CJ and TJ; methodology, TJ; software, LY; validation, LY and WS; formal analysis, CJ; investigation, LY; resources, WS; data curation, LY; writing—original draft preparation, CJ; writing—review and editing, WJ; visualization, LY; supervision, LT; project administration, TJ; funding acquisition, TJ. All authors have read and agreed to the published version of the manuscript.

Funding: This research was funded by the Program for Guangdong Introducing Innovative and Entrepreneurial Teams. (Project number: 2017ZT07S225).

Conflict of interest: The authors declare no conflict of interest.

References

1. Wei J, Chen H, Chen Y, et al. China Spallation Neutron Source: Design, R&D, and outlook. Nuclear Instruments and Methods in Physics Research Section A: Accelerators, Spectrometers, Detectors and Associated Equipment. 2009; 600(1): 10-13. doi: 10.1016/j.nima.2008.11.017
2. Chen Y. China Spallation Neutron Source (CSNS). Bulletin of Chinese Academy of Sciences. 2011; 26(6): 726-728.
3. Wang F, Liang T, Yin W, et al. Conceptual design of target station and neutron scattering spectrometers for the Chinese spallation neutron source. Nuclear techniques. 2005; 8: 593-597. doi: 10.3321/j.issn:0253-3219.2005.08.006
4. Haines JR, McManamy TJ, Gabriel TA, et al. Spallation neutron source target station design, development, and commissioning. Nuclear Instruments and Methods in Physics Research Section A: Accelerators, Spectrometers, Detectors and Associated Equipment. 2014; 764: 94-115. doi: 10.1016/j.nima.2014.03.068
5. Ikeda Y. Scientific Reviews: 1-MW Pulse Sapllation Neutron Source (JSNS) of J-PARC. Neutron News. 2005; 16(1): 20-24. doi: 10.1080/10448630500454189
6. Bauer GS, Salvatores M, Heusener G. MEGAPIE, a 1 MW pilot experiment for a liquid metal spallation target. Journal of Nuclear Materials. 2001; 296(1): 17-33. doi: 10.1016/S0022-3115(01)00561-X
7. Aguilar A, Sordo F, Mora T, et al. Design specification for the European Spallation Source neutron generating target element. Nuclear Instruments and Methods in Physics Research Section A: Accelerators, Spectrometers, Detectors and Associated Equipment. 2017; 856: 99-108. doi: 10.1016/j.nima.2017.03.003
8. Burns GJ, Dey A, Findlay DJS, et al. Erosion of neutron-producing targets at ISIS spallation neutron source. Nuclear Instruments and Methods in Physics Research Section B: Beam Interactions with Materials and Atoms. 2022; 521: 7-16. doi: 10.1016/j.nimb.2022.04.004
9. Wei S, Zhang R, Shi Y, et al. Development of CSNS Target. Atomic Energy Science and Technology. 2019; 53(12): 2441-2446. doi: 10.7538/yzk.2018.youxian.0885
10. Futakawa M, Kogawa H, Hino R, et al. Erosion damage on solid boundaries in contact with liquid metals by impulsive pressure injection. International Journal of Impact Engineering. 2003; 28(2): 123-135. doi: 10.1016/S0734-743X(02)00054-4
11. Park JJ, Butt DP, Beard CA. Review of liquid metal corrosion issues for potential containment materials for liquid lead and lead-bismuth eutectic spallation targets as a neutron source. Nuclear Engineering and Design. 2000; 196(3): 315-325. doi: 10.1016/S0029-5493(99)00303-9
12. Hao J, Chen Q, Lu Y, et al. Thermal Design of a Spallation Neutron Source Target System. Journal of Engineering Thermophysics. 2013; 34: 1515-1518.
13. Hao J, Chen Q, Xu Y, et al. Flow field optimization and design for a Spallation Neutron Source target cooling system. Science China Technological Sciences. 2013; 56(6): 1370-1376. doi: 10.1007/s11431-013-5215-4
14. Lu Y, Tong J, Wang S, et al. The influence of proton beam offset on CSNS target heat transfer performance. In: Proceedings for the 14th National Conference on Reactor Thermalhydraulics; 23 September 2015; Beijing, China.
15. Takenaka N, Nio D, Kiyanagi Y, et al. Thermal hydraulic design and decay heat removal of a solid target for a spallation neutron source. Journal of Nuclear Materials. 2005; 343(1-3): 169-177. doi: 10.1016/j.jnucmat.2004.11.017
16. Bauer GS. Overview on spallation target design concepts and related materials issues. Journal of Nuclear Materials. 2010; 398(1-3): 19-27. doi: 10.1016/j.jnucmat.2009.10.005

17. Li Y, Roux S, Castelain C, et al. Tailoring the fluid flow distribution in a parallel mini-channel heat sink under multiple-peak heat flux. Thermal Science and Engineering Progress. 2022; 29: 101182. doi: 10.1016/j.tsep.2021.101182
18. Kumar S, Singh PK. A novel approach to manage temperature non-uniformity in minichannel heat sink by using intentional flow maldistribution. Applied Thermal Engineering. 2019; 163: 114403. doi: 10.1016/j.applthermaleng.2019.114403